

# Optimal filtering of optical and weak lensing data to search for galaxy clusters: application to the COSMOS field

F. Bellagamba<sup>1</sup>, M. Maturi<sup>2</sup>, T. Hamana<sup>3</sup>, M. Meneghetti<sup>4,5</sup>, S. Miyazaki<sup>3</sup>,  
L. Moscardini<sup>1,5</sup>

<sup>1</sup>*Dipartimento di Astronomia, Università di Bologna, Via Ranzani 1, 40127, Bologna, Italy*

<sup>2</sup>*Zentrum für Astronomie, ITA, Universität Heidelberg, Albert-Ueberle-Str. 2, 69120, Heidelberg, Germany*

<sup>3</sup>*National Astronomical Observatory of Japan, Mitaka, Tokyo 181-8588, Japan*

<sup>4</sup>*INAF-Osservatorio Astronomico di Bologna, Via Ranzani 1, 40127, Bologna, Italy*

<sup>5</sup>*INFN-National Institute for Nuclear Physics, Sezione di Bologna, Viale Berti Pichat 6/2, 40127, Bologna, Italy*

## ABSTRACT

Galaxy clusters are usually detected in blind optical surveys via suitable filtering methods. We present an optimal matched filter which maximizes their signal-to-noise ratio by taking advantage of the knowledge we have of their intrinsic physical properties and of the data noise properties. In this paper we restrict our application to galaxy magnitudes, positions and photometric redshifts if available, and we also apply the filter separately to weak lensing data. The method is suitable to be naturally extended to a multi-band approach which could include not only additional optical bands but also observables with different nature such as X-rays. For each detection, the filter provides its significance, an estimate for the richness and for the redshift even if photo- $z$  are not given. The provided analytical error estimate is tested against numerical simulations. We finally apply our method to the COSMOS field and compare the results with previous cluster detections obtained with different methods. Our catalogue contains 27 galaxy clusters with minimal threshold at 3-sigma level including both optical and weak-lensing information.

**Key words:** cosmology: theory – cosmology: observations – large scale structure of the Universe – galaxies: clusters: general – galaxies: luminosity function, mass function – gravitational lensing: weak

## 1 INTRODUCTION

Clusters of galaxies lie in the densest regions of the Universe. In the standard  $\Lambda$ CDM model, they form from the highest peaks of the primordial density fluctuations. Their abundance as a function of mass and redshift is an extremely important tool to determine cosmological parameters and the history of structure formation. It is therefore fundamental to build robust tools to detect galaxy clusters in different observational bands.

In optical surveys, clusters of galaxies can be successfully identified via overdensities of galaxies with respect to the mean field and via the coherent distortion of background galaxies due to gravitational lensing. These two observables come together with the same data but have very different properties. On one hand lensing analyses have the advantage of directly mapping dark matter structures, but to be performed they need high-quality imaging data, and their results are intrinsically very noisy. On the other hand, detecting clusters through galaxy overdensities is much less

demanding from an observational point of view, because it does not require any shape measurement. Moreover, if an optical cluster finding is performed on a lensing survey field, it can be used as a useful tool to eliminate spurious detections.

A common approach in lensing is to convolve galaxy ellipticities with a suitable filter to find the cluster signal beyond the noise induced by intrinsic ellipticity of galaxies and cosmic shear by large-scale structures. Different filters have been proposed so far, including the Gaussian filter (Miyazaki et al. 2002), the aperture mass in the version of Schneider et al. (1998), its modifications by Schirmer et al. (2004), and the one proposed by Hennawi & Spergel (2005). Maturi et al. (2005) proposed an optimal filter, which minimizes noises due to both the intrinsic ellipticity and the cosmic shear, selecting the scales on which the cluster signal-to-noise ratio is expected to be maximum. A comparison of the performance of the different filters used to find dark matter halos in cosmological simulations has been presented in Pace et

al. (2007). An application to GaBoDs data of the optimal filter is in Maturi et al. (2007).

The idea of this work is to apply the linear filtering technique to optical galaxy catalogues, possibly accounting for 3D information, if available through photometric redshifts, to perform a combined analysis of galaxy overdensities and weak lensing data.

To build an optimal linear filter for galaxy overdensities, we start from the pioneering approach proposed by Postman et al. (1996), who developed an optical filter to analyse the data of the Palomar Distant Cluster Survey. Many authors have proposed different modifications of the original Postman filter: for example Kepner et al. (1999) introduced Poisson (instead of the Gaussian) statistics and a rough usage of photometric redshifts; Dong et al. (2008) allowed the radius of the filter to change to adapt to the detected signal; Milcraitis et al. (2009) tuned the parameters using mock light-cones extracted from the Millennium Simulation (Springel et al. 2005).

In this work, we construct a Postman-like filter as a linear filter, using the estimated richness of the cluster and not the likelihood of the data as main object of analysis. This allows us to keep the linearity with respect to the galaxy density and to calculate an error estimate analytically. We also introduce the information from photometric redshifts in the procedure. We apply the filter to some simulated catalogues to verify the consistency of the error estimates and to assess the reliability of the cluster redshift determination obtained with our algorithm, even when galaxy photometric redshifts are not available. The final step of this work is then the application of both optimal filtering algorithms (for optical and weak lensing data) to the COSMOS field (Scoville et al. 2007a). Previous cluster detections on the same field were done by Finoguenov et al. (2007) combining optical and X-ray information, by Olsen et al. (2007) and Scoville et al. (2007b) from optical data only, and by Kasliwal et al. (2008) and Miyazaki et al. (2007) via lensing analyses.

The paper is organized as follows. In Section 2, we show the idea, the mathematical derivation and our implementation of the filter. We also describe how to derive a redshift estimate for the detected galaxy clusters, both with and without the information coming from photometric redshifts. In Section 3, we investigate the filter properties and test the algorithm using numerical simulations. In Section 4, we briefly summarize the properties of the optimal filter for weak lensing detections, highlighting the similarities with the optical filter. In Section 5, we apply both algorithms to galaxy catalogues from the COSMOS survey and we discuss the resulting cluster detections. We compare these results with previous cluster catalogues obtained with different techniques on the same field. Summary, conclusions and future prospects of this work are provided in Section 6.

## 2 OPTIMAL FILTER FOR GALAXY OVERDENSITIES

To derive the optimal filter, we assume that positions, magnitudes (at least in one band), and possibly photometric redshifts of the galaxies in a surveyed field are available. Furthermore, we assume that bound structures like galaxy clusters present in the field can be traced by the galaxy dis-

tributions within them and that the spatial distribution of background galaxies is random. Under these assumptions, given the characteristics of the survey, bands of observation and depth, it is possible to define a cluster model, describing the expected spatial and magnitude distributions of the cluster galaxies and a noise model describing the background distribution of field galaxies.

Thus we define a model  $n_m(\boldsymbol{\theta}, m)$  for the observed distribution of galaxies as a function of the position  $\boldsymbol{\theta}$  and magnitude  $m$ , given by the sum of a field and a cluster component (Postman et al. 1996):

$$n_m(\boldsymbol{\theta}, m) = n_f(m) + \Lambda n_c(\boldsymbol{\theta}, m) = n_f(m) + \Lambda P(\boldsymbol{\theta} - \boldsymbol{\theta}_c) \phi(m), \quad (1)$$

where  $n_f(m)$  is the magnitude distribution of field galaxies,  $\boldsymbol{\theta}_c$  is the cluster centre,  $P$  is the projected radial profile of the cluster galaxies number density,  $\phi(m)$  is the cluster luminosity function and  $\Lambda$  is a richness parameter, proportional to the total number of cluster galaxies.

The detection of a cluster in the input catalogue is based on the comparison of the observed distribution of galaxies to the model  $n_m$ . More specifically, for a fixed cluster centre  $\boldsymbol{\theta}_c$ , we compute the value of  $\Lambda$  for which our model distribution best describes the observed distribution  $n_d(\boldsymbol{\theta}, m)$ . The likelihood of the observed data  $n_d$  given the model  $n_m$  is

$$\begin{aligned} \mathcal{L} &= - \int \frac{[n_d(\boldsymbol{\theta}, m) - n_m(\boldsymbol{\theta}, m)]^2}{n_m(\boldsymbol{\theta}, m)} d\Omega dm \\ &= - \int \frac{[n_d(\boldsymbol{\theta}, m) - n_f(m) - \Lambda n_c(\boldsymbol{\theta}, m)]^2}{n_f(m)} d\Omega dm, \quad (2) \end{aligned}$$

assuming that the background noise is Poissonian noise and that the galaxy density is high enough such that the Gaussian approximation holds.

We derive the value of the richness  $\Lambda$  that maximizes  $\mathcal{L}$  by imposing

$$\frac{d\mathcal{L}}{d\Lambda} = 2 \int \frac{n_c}{n_f} (n_d - n_f) d\Omega dm - 2\Lambda \int \frac{n_c^2}{n_f} d\Omega dm = 0, \quad (3)$$

which leads to

$$\begin{aligned} \Lambda &= \frac{\int \frac{n_c}{n_f} (n_d - n_f) d\Omega dm}{\int \frac{n_c^2}{n_f} d\Omega dm} \\ &= \frac{\int \frac{n_c}{n_f} n_d d\Omega dm - \int n_c d\Omega dm}{\int \frac{n_c^2}{n_f} d\Omega dm}. \quad (4) \end{aligned}$$

Only the first term in the numerator depends on the spatial distribution of the data with respect to  $\boldsymbol{\theta}_c$ . Thus, Equation (4) can be re-written as

$$\Lambda = \int \Phi(\boldsymbol{\theta} - \boldsymbol{\theta}_c, m) n_d(\boldsymbol{\theta}, m) d\Omega dm - B, \quad (5)$$

where  $\Phi$  is the optical linear filter defined as

$$\Phi(\boldsymbol{\theta} - \boldsymbol{\theta}_c, m) = \left( \int \frac{n_c^2}{n_f} d\Omega dm \right)^{-1} \frac{n_c(\boldsymbol{\theta}, m)}{n_f(m)}, \quad (6)$$

and  $B$  is the contribution of background galaxies that is subtracted to work on a zero-mean noise field,

$$B = \left( \int \frac{n_c^2}{n_f} d\Omega dm \right)^{-1} \int n_c d\Omega dm. \quad (7)$$

If we insert  $\Lambda$  obtained from Equation (4) back into Equation (2), we obtain the corresponding value of the likelihood

$$\mathcal{L} = \mathcal{L}_0 + \frac{\left[ \int \frac{n_c}{n_f} (n_d - n_f) d\Omega dm \right]^2}{\int \frac{n_c^2}{n_f} d\Omega dm}, \quad (8)$$

where  $\mathcal{L}_0$  is a (negative) constant that does not depend on the position of the cluster  $\theta_c$ . Comparing Equations (8) and (4), we see that the varying part of  $\mathcal{L}$  is proportional to  $\Lambda^2$ . This squared dependence of  $\mathcal{L}$  on  $\Lambda$  reflects the fact that the  $\chi^2$  approach returns high likelihoods also for galaxy underdensities, for which  $\Lambda$  would be negative.

This is why we consider convenient to search for galaxy clusters as peaks of the distribution of  $\Lambda$  as a function of the sky position  $\theta_c$ , instead of likelihood maxima. In fact, we take full advantage of the linear response to the data, provided by Equation (5), and of the physical direct interpretation of  $\Lambda$ , which is a suitably normalized number of visible galaxies belonging to the cluster (see Section 2.1).

The variance of  $\Lambda$  is given by  $\sigma_\Lambda^2 \equiv \langle (\Lambda - \hat{\Lambda})^2 \rangle$ , where  $\hat{\Lambda}$  is an estimate of the true value of  $\Lambda$ , given by Equation (5). Since  $\Lambda \hat{n}_c(m, \theta)$  and  $\hat{n}_f(m)$  are random realizations of the cluster and field populations, the resulting  $\sigma_\Lambda^2$  has two contributions: the first term is induced by the random fluctuations in the background, the second by the random sampling of the cluster model:

$$\sigma_\Lambda^2 = \left( \int \frac{n_c^2}{n_f} d\Omega dm \right)^{-1} + \Lambda \frac{\int \frac{n_c^3}{n_f^2} d\Omega dm}{\left( \int \frac{n_c^2}{n_f} d\Omega dm \right)^2}. \quad (9)$$

By applying the formalism of linear matched filters, one can see that the filter minimizes the variance of the estimated  $\Lambda$  due to random fluctuations only. The second term in Equation (9) gives the intrinsic Poissonian fluctuation of the cluster realization.

## 2.1 Modelling the galaxy clusters

The cluster optical model is specified by the spatial and luminosity distribution of cluster galaxies. For simplicity, we assume spherical symmetry. We also assume that the projected radial distribution of the cluster members follows an NFW model (Navarro et al. 1997; Bartelmann 1996; Meneghetti et al. 2002):

$$\Sigma(x) = \frac{2\rho_s r_s}{x^2 - 1} f(x), \quad (10)$$

with

$$f(x) = \begin{cases} 1 - \frac{2}{\sqrt{x^2 - 1}} \arctan \sqrt{\frac{x-1}{x+1}} & (x > 1) \\ 1 - \frac{2}{\sqrt{1-x^2}} \operatorname{arctanh} \sqrt{\frac{1-x}{1+x}} & (x < 1) \\ 0 & (x = 1) \end{cases},$$

where  $x \equiv r/r_s$ . This distribution, apart from the normalization  $\rho_s$ , depends on the scale radius  $r_s$  only, corresponding to  $R_{200}/c$ , where  $R_{200}$  is the scale where the galaxy density is 200 times the critical density, and  $c$  is the so-called concentration parameter. Our choice is motivated by the analysis made by Hansen et al. (2005) on a large sample of

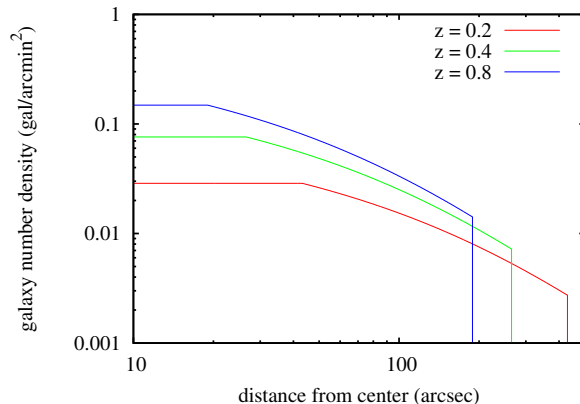


**Figure 1.** Radial profiles of the cluster model at different redshifts, as labelled in the figure. **The profile is flattened inside 100 Kpc/h to avoid the central divergence, while the cut off at large radius corresponds to the  $R_{200}$  limit.**

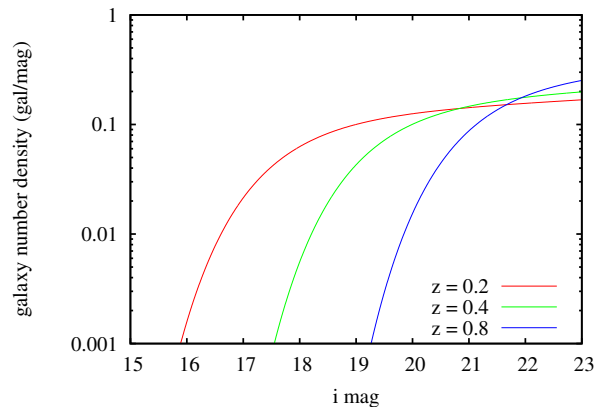


**Figure 2.** Magnitude functions of the cluster model at different redshifts, as labelled in the figure.

optically-selected clusters from the SDSS. They found that the NFW model is a good description of the cluster galaxy distribution up  $R_{200}$ . The concentration parameters derived from galaxy distributions described by the NFW model depends on the richness but it is in general smaller ( $1 < c < 3$ ) than those found in numerical simulations for dark matter halos of similar mass. In this context we use a scale radius  $r_s = 500$  kpc/h, that represents a good estimate for quite rich clusters (see Figs. 7 and 8 in Hansen et al. 2005). The resulting radial profiles computed at different redshifts are shown in Fig. 1, as examples.

For the cluster luminosity distribution, we assume the Schechter luminosity functions (Schechter 1976), with parameters taken from Popesso et al. (2005), who analysed 97 clusters observed in the SDSS. Since these are calculated from galaxy counts inside a radius of 1 Mpc/h from the cluster centre, we apply the same cut to the radial density profile. For a realistic concentration parameter  $c = 2$ , this implies that we limit our analysis within  $R_{200}$ , where the projected NFW is a good description of observed clusters, as discussed.

Apart from the cluster model, the other ingredient of our recipe is the distribution of field galaxies, that we assume to be random with a fixed mean angular number density. The magnitude distribution of the field galaxies  $n_f(m)$  can be estimated from the distribution of the whole galaxy sample, provided that the field is large enough such that the contribution of cluster galaxies can be considered negligible.

## 2.2 Map making

Clusters are searched in three-dimensional space, where their positions are given by the angular coordinates  $\theta_c$  and by the redshift  $z_c$ . We create maps of  $\Lambda$  estimates for different values of the redshift, and we search for cluster detections in these maps. Comparison of detections in different redshift slices is done subsequently (see Section 2.3.1).

For every redshift, we adapt the cluster model  $n_c$  in a proper way. First, we transform the cluster absolute luminosity function into an apparent magnitude distribution (see Fig. 2), and re-scale the radial profile of the cluster model according to the angular-diameter distance. Then, we normalize properly the cluster model  $n_c$  to set the richness parameter  $\Lambda$  to be the total number  $N$  of visible galaxies in a cluster. Integrating the cluster model, we get:

$$N = \Lambda \int n_c(\theta, m) d^2\theta dm \quad (11)$$

$$= \Lambda \iint P(\theta) d^2\theta \int \phi(m) dm. \quad (12)$$

To set  $N = \Lambda$ , we impose the integrals of the angular distribution and the luminosity function to be normalized to unity, that is

$$\iint P(\theta) d^2\theta = 1, \quad (13)$$

$$\int_0^{m_{\text{lim}}} \phi(m) dm = 1, \quad (14)$$

where  $m_{\text{lim}}$  is the limiting magnitude of the sample.

At a fixed redshift  $z_c$ , we build a two-dimensional map evaluating  $\Lambda$  over a grid of angular positions  $\theta_c$ . Since we deal with discrete quantities, the integral in Equation (4) must be approximated as a sum over the galaxy positions. Only the first term in the numerator needs to be evaluated for every grid position  $\theta_c$ , while the second one is equal to unity because of the normalization. The denominator for a given redshift is a constant for all sky positions. We denote it by  $C$ . Thus the discretized version of Equation (4) reduces to

$$\Lambda_{ij} = \Lambda(\theta_i, \theta_j) = \frac{A_{ij} - 1}{C}, \quad (15)$$

where

$$A_{ij} = \sum_{k=1}^N \frac{n_c(r_k, m_k)}{n_f(m_k)} = \sum_{k=1}^N \frac{P(r_k)\phi(m_k)}{n_f(m_k)}. \quad (16)$$

In the formula above,  $r_k$  is the angular distance of the galaxy from the centre

$$r_k = |\theta_k - (\theta_i, \theta_j)|, \quad (17)$$

and the index  $k$  runs over all  $N$  galaxies of the sample. Clusters candidates are identified with the peaks of the resulting  $\Lambda$ -map. To select only significant peaks, we calculate their

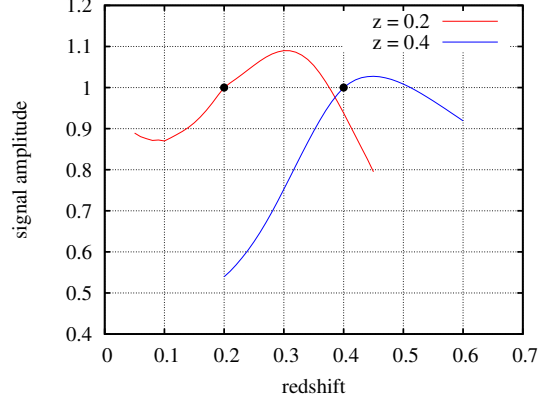


**Figure 3.** Analytic response of the algorithm (Eq. 18) for two clusters at redshifts 0.2 and 0.4. When the cluster is seen at the correct redshift, the value of the response is unity by definition (black points).

signal-to-noise ratios using the variance given in Equation (9).

## 2.3 Redshift determination

### 2.3.1 Without photometric redshifts

To estimate the cluster redshift, we cannot just maximize  $\Lambda$  with respect to  $z_c$ . Indeed, this would introduce a bias as discussed below. The analytic response of the algorithm as a function of the search redshift  $z_c$  for a cluster at a redshift  $\bar{z}_c$  and with a galaxy distribution  $\bar{n}_c$  is

$$\Lambda(z_c) = \frac{\int \frac{n_c}{n_f} \bar{n}_c d\Omega dm}{\int \frac{n_c^2}{n_f} d\Omega dm}. \quad (18)$$

This corresponds to Equation (4) when applied to a known distribution  $n_d = n_f + \bar{n}_c$ . By construction,  $\Lambda = 1$  when  $z_c = \bar{z}_c$ , but there is no reason why this should be a maximum for the function  $\Lambda(z_c)$ . This is shown in Fig. 3, where we plot the analytic response for two clusters located at  $z = 0.2$  and  $z = 0.4$ . For both of them the maximum of  $\Lambda$  as a function of  $z_c$  is found at a higher redshift than the cluster's.

For a correct redshift estimate, the likelihood  $\mathcal{L}$  (Equation 8) in the peaks of the 2D distribution of  $\Lambda$  must be used. By definition, the value of  $\mathcal{L}$  is maximal when the cluster is filtered by a model at the correct redshift (See Fig. 4).

### 2.3.2 With photometric redshifts

If the photometric redshift is available for each galaxy, we can use this further information in our analysis. Assuming that a redshift probability distribution  $p_k(z)$  is derived for the  $k$ -th galaxy of the sample,  $p_k(z_c)$  can be used as a weight factor for that galaxy when estimating the field number density,  $n_f$ , the cluster richness,  $\Lambda$ , and the likelihood,  $\mathcal{L}$ , at a redshift  $z_c$ .

On the other hand, this can be interpreted as an extension of the two-dimensional linear matched filter to a

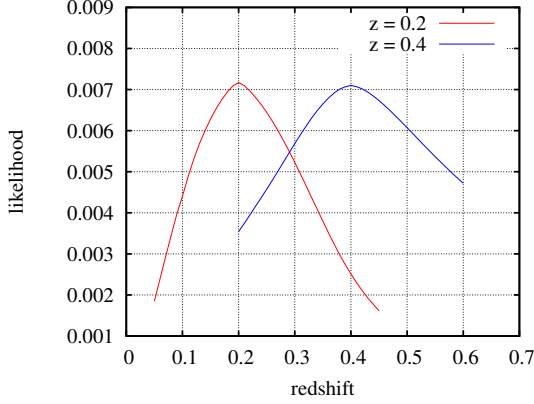


**Figure 4.** Analytic value of  $\mathcal{L}$  for two clusters at redshift 0.2 and 0.4, as a function of the search redshift  $z_c$ .

three-dimensional one, where the redshift probability function represents the cluster profile along the line of sight. In fact, in an ideal case where all galaxies have the same redshift probability distribution, which for simplicity we assume to be a Gaussian distribution centered on their most probable location,  $z_{est,k}$ , with a constant rms,  $\sigma_z$ ,

$$p_k(z) = \frac{1}{\sqrt{2\pi}\sigma_z} \exp\left(-\frac{(z_{est,k} - z)^2}{2\sigma_z^2}\right), \quad (19)$$

the three-dimensional model with a cluster at redshift  $z_c$  is

$$\begin{aligned} n_m(\boldsymbol{\theta}, m, z) &= n_f(m, z) + \Lambda n_c(\boldsymbol{\theta}, m, z) \\ &= n_f(m, z) + \Lambda P(\boldsymbol{\theta} - \boldsymbol{\theta}_c) \phi_z(m) p(z), \end{aligned} \quad (20)$$

where

$$p(z) = \frac{1}{\sqrt{2\pi}\sigma_z} \exp\left(-\frac{(z_c - z)^2}{2\sigma_z^2}\right). \quad (21)$$

If we then further assume that the background distribution is only slowly changing with redshift, so that the background  $n_f(m, z)$  for  $z_c - \sigma_z < z < z_c + \sigma_z$  is constant, the richness estimate at redshift  $z_c$  is

$$\Lambda = \frac{\int \frac{n_c(\boldsymbol{\theta}, m, z)}{n_f(m, z_c)} (n_d(\boldsymbol{\theta}, m, z) - n_f(m, z_c)) d\Omega dm dz}{\int \frac{n_c^2(\boldsymbol{\theta}, m, z)}{n_f(m, z_c)} d\Omega dm dz}. \quad (22)$$

This is equivalent to Equation (4), but with the additional dimension. In practical applications, Equation (22) has to be discretized in analogy with Equation (15). Thus,

$$A_{ij} = \sum_{k=1}^N \frac{P(r_k) \phi(m_k) p_k(z_c)}{n_f(m_k, z_c)}. \quad (23)$$

In this case the numerator is evaluated weighting every galaxy with  $p_k(z_c)$ . The constant denominator  $C$ , that does not depend on the observed galaxy spatial distribution, can be evaluated using a model for  $\sigma_z$ , possibly depending on the magnitude and the redshift estimate of the galaxies. The same model is also necessary for the evaluation of the variance that, in analogy with Equation 9, is

$$\sigma_\Lambda^2 = \left( \int \frac{n_c^2}{n_f} d\Omega dm dz \right)^{-1} + \Lambda \frac{\int \frac{n_c^3}{n_f^2} d\Omega dm dz}{\left( \int \frac{n_c^2}{n_f} d\Omega dm dz \right)^2}. \quad (24)$$

In the process of estimating the redshift from multi-band photometry, a spectral type is also assigned to each galaxy. This can be used to k-correct the values of the magnitude and to obtain rest-frame values, which are directly comparable to the model. The filter is applied to the data as usual, creating maps for different redshift slices and selecting peaks, as described in Section (2.2). The most likely redshift estimate for a detection is then chosen.

## 2.4 Comparison with other optical cluster finding methods

The optimal matched filter we used for cluster detections (both optical and weak lensing) relies on the general knowledge we have of galaxy clusters, as incorporated in the cluster model, and selects all physical properties which enables us to distinguish them from the field. It is in fact a general approach which can incorporate at once different cluster aspects in contrast to other methods which aim at a single signature such as galaxy overdensities, cluster galaxy redsequence, cD galaxies, etc. In other words, instead of enforcing some criteria which is later applied to data, we first define the general properties of galaxy clusters and then let the filter find what are the distinctive features for their detection given the actual data noise.

In the following sections we discuss the main techniques applied in literature and how they compare with the one presented in this work.

### 2.4.1 Galaxy overdensities

Looking for galaxy overdensities in astronomical images by eye was the first method used to detect galaxy clusters. In the last decades different automated methods were proposed, such as friend-of-friend algorithms (Li & Yee 2008), Voronoi tessellation (Ramella et al. 2001), filtering by wavelets (Finoguenov et al. 2007), adapting kernels (Mazure et al. 2007) or matched filters (e.g. Postman et al. 1996; Kepner et al. 1999; Gilbank et al. 2004; Dong et al. 2008; Menanteau et al. 2009; Milkeraitis et al. 2009). Together with the additional features discussed in the following sections, our algorithm incorporates the mentioned matched filters. In fact it includes the angular clustering information on the sky according to the  $P$  term of Equation (23) or, if photometric redshifts are available, the full three-dimensional clustering information thanks to the  $p$  term of Equation (23). In more details, the main differences with respect to the matched filters mentioned in this section are:

(i) our filter can take advantage of the information from photometric redshifts in a very flexible way, accounting for their uncertainty. Instead of simply slicing the data-set and neglecting all galaxies outside a fixed redshift range (e.g. Milkeraitis et al. 2009), we consider all galaxies belonging to the data set by weighing them according to their own redshift probability distribution.

(ii) It uses distinct luminosity functions for galaxy clusters and field galaxies to define the cluster model and the noise contribution. Although this seems an obvious choice, previous filtering algorithms use the luminosity functions taken from the whole population of galaxies, including the field, to define the cluster model.

(iii) It is linear with respect to the data, because it makes use of the richness  $\Lambda$  instead of the likelihood  $\mathcal{L}$  as the main object of analysis. In fact, even if they are based on the same statistical distribution,  $\Lambda$  is linear, in contrast with  $\mathcal{L}$  which is quadratic, and therefore is capable to distinguish positive overdensities from negative underdensities to which  $\mathcal{L}$  would assign high probabilities.

(iv) It gives as a natural output an estimate of the number of observed galaxies in a cluster, which can be easily corrected for redshift dimming to get a meaningful physical quantity (see Section 5.1).

#### 2.4.2 Brighter cluster galaxy

The algorithm used by Koester et al. (2007), based mainly on red-sequence information, includes a cut-off term for the brighter cluster galaxy luminosity, such that detections without a very brilliant central galaxy are discarded. In our approach, instead of looking for a specific cluster member, we let the filter select in an optimal way the whole luminosity function  $\phi$  expected for a cluster at a given redshift in contrast with the field luminosity function  $n_f$ , as in Equation (23). As the most massive and luminous galaxies are found preferably at the center of the clusters, at low magnitudes the ratio between the cluster model luminosity function and the observed field distribution will increase. The algorithm will assign large weights to very luminous galaxies and thus they will be a strong indication of the presence of clusters. The advantage of our approach is that the filter is defined according to well defined statistical quantities and not to a free parameter. In addition we allow the algorithm to be sensitive to a broad range of systems, from rich clusters to groups which might otherwise fall below a given threshold.

#### 2.4.3 Cluster galaxies red sequence

Red-sequence cluster finders rely on the fact that the center of galaxy clusters is typically populated by elliptical galaxies whose color is on average redder than the one of the field galaxies at the same redshift. Usually a cut in a colour-magnitude diagram is performed to select these red galaxies overdensities that identify the galaxy cluster candidates. This technique, presented in Gladders & Yee (2000), has been successfully used in different galaxy surveys (e.g. Gladders & Yee 2005; Koester et al. 2007; Lu et al. 2009; Thanjavur et al. 2009). We thus mention and explain how this technique can be implemented in the framework of our method with a simple generalization, even if we did not explicitly make use of color information in this work. In a following paper we will fully discuss a multi-band approach which deserves an extended discussion on its own.

Our method belongs to the matched filters developed for CMB observations (e.g. Schäfer et al. 2001; Pace et al. 2008) which use at once all available bands to obtain a unique response. With this respect, the algorithm presented here is a

special case where a single band is considered, but could be naturally extended to include the full available color information. In this way, we would consider not only the two bands that are usually used in classical red-sequence searches, but all bands and color properties of the clusters and the field, adding new possible information. Again, this would be done not by defining a cut-off in the color space but by defining the proper weight to each galaxy performing an optimized analysis.

In any case, already at this stage without multi-band information, we partially account for the massive galaxies, as those targeted more precisely by the red sequence, thanks to the use of the cluster luminosity function (see Section 2.4.2).

### 3 INVESTIGATING THE FILTER PROPERTIES

The final step of this work will be the application of the algorithm to real data, namely the  $i'$  band galaxy catalogue of the COSMOS field (Ilbert et al. 2009), limited at  $i' = 25$ . Before doing this, we have to evaluate the capability of our algorithm to detect clusters and to correctly measure their richness and redshift. In these tests we use the field distributions measured from the COSMOS data to define the filter. Thus, we use the specific implementation of the algorithm that will be later adopted for the final data analysis.

#### 3.1 Signal-to-noise estimates

We now evaluate the expected signal-to-noise ratios for clusters with different redshift and richness, as described by our cluster model, once the actual properties of the galaxies in the COSMOS catalogue are assumed. The expected signal-to-noise ratios when the photometric redshifts are neglected are shown in the upper panel of Fig. 5. In this case, the expected signal and noise are given by Equations (4) and (9), respectively, and the signal-to-noise ratio peaks at  $z \sim 0.45$ . To explain this behaviour, we plot separately in Fig. 6 the expected signal of a cluster with 100 visible galaxies at  $z = 0.2$  and the two noise terms as a function of redshift. The signal, i.e. the number of visible galaxies of the modeled cluster, decreases for increasing  $z$  as expected (solid line). The trend for the noise is different: on one hand, the term related to the background galaxies only (dot-dashed line) grows monotonically as a function of redshift up to  $z \sim 0.5$  after which it basically stays constant; on the other hand, the intrinsic fluctuations of the cluster signal decreases monotonically with  $z$ . As a result the latter term is dominant at low redshifts (up to  $z \lesssim 0.4$ ).

This noise behaviour derives from the fact that for low-redshift clusters, the filter, being proportional to  $n_c(m)/n_f(m)$ , selects the bright end of the cluster luminosity function, that has almost no background. Therefore the background noise decreases with redshift while the intrinsic fluctuations of the cluster signal increase because the  $\Lambda$  estimate depends in practice on the very few bright galaxies only.

In order to consider the case in which photometric redshift information is available, we use the values for the redshift ( $z_{est}$ ) and its 68% confidence levels ( $z_{min}$ ,  $z_{max}$ ) re-

ported in the COSMOS catalogue to associate to each galaxy a probability distribution given by

$$p(z) = \frac{1}{\sqrt{2\pi}\sigma_m} \exp\left(-\frac{(z - z_{est})^2}{2\sigma^2}\right), \quad (25)$$

where

$$\sigma = \begin{cases} z_{est} - z_{min} & \text{if } z < z_{est} \\ z_{max} - z_{est} & \text{if } z > z_{est} \end{cases}, \quad (26)$$

and

$$\sigma_m = (z_{max} - z_{min})/2. \quad (27)$$

When estimating the normalization constants, i.e. the denominator of Equation (22) and the variance (Equation 24), which do not depend on the observed spatial galaxy distribution, we use the mean redshift error for different classes of objects, estimated from the comparison with a spectroscopic subsample (Ilbert et al. 2009). For our dataset, these errors are:

$$\sigma_{\Delta z/1+z} = \begin{cases} 0.007 & \text{for } 0.2 < z < 1.5, \quad i' < 22.5 \\ 0.011 & \text{for } 0.2 < z < 1.5, \quad 22.5 < i' < 24 \\ 0.053 & \text{for } 0.2 < z < 1.5, \quad 24 < i' < 25 \\ 0.06 & \text{for } z > 1.5 \end{cases}. \quad (28)$$

As we can see in the lower panel of Fig. 5, using the photo- $z$  information, the picture becomes more confused, as the sensitivity depends on the field population density  $n_f(m, z)$  at the search redshift (see Equation 24). The only clear trend is the decrement of the sensitivity at high redshift due to the dimming of the cluster signal. In this case we do not have any worsening of the performance at low redshift because the weight given by the filter through the  $n_c(m)/n_f(m, z)$  ratio selects almost the same part of the luminosity function at each redshift.

### 3.2 Simulations with mock catalogues

We then test the application of our algorithm to mock galaxy catalogues, built from the COSMOS data. To create realistic catalogues for the field galaxies, we first randomize the positions of the galaxies to cancel any structures contained in the field. We assume that the cluster galaxies do not affect the photometric properties of the overall sample because their number is negligible with respect to that of the field galaxies. On the top of this random background, we add some mock clusters. The cluster galaxies are distributed according to the model for the spatial and luminosity distribution of the cluster members (see Section 2.1). The photometric redshifts are assigned following a Gaussian redshift probability distribution with errors given by Equation (28). For illustrative purposes, we first generate a square field with side 1 degree, containing 25 galaxy clusters of different richness and redshift placed on a regular grid. In Fig. 7 we show the results of the analysis of this field without the usage of photometric redshifts, at a search redshift  $z_c = 0.4$ . All clusters leave an imprint on the  $\Lambda$ -map, whose strength depends on the richness and the redshift, with clusters at  $z = z_c$  being brighter than the others with the same  $\Lambda$ .

Other simulations are done to verify the linear response of the filter with respect to the cluster richness. In this case, we assume for simplicity all clusters at  $z = 0.4$  and compare the input number of galaxies to the estimated one. The

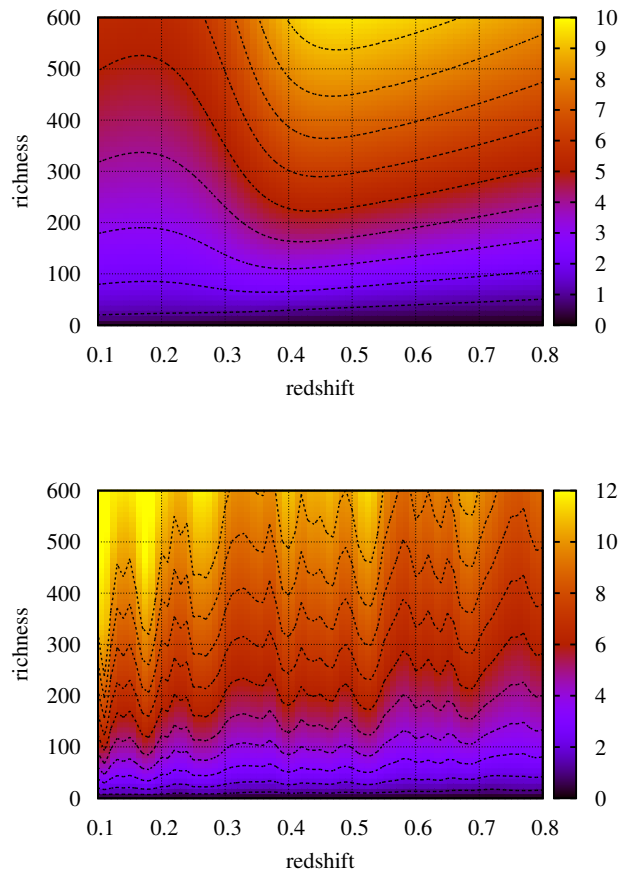


**Figure 5.** Expected signal-to-noise values for the detection of a cluster, without (top panel) and with (bottom panel) photometric redshifts, for the COSMOS  $i'$  band catalogue. The black contours refer to different integer values for S/N, starting from unity at the bottom (see the color bar on the right). The value on the y-axis is the number of galaxies of the cluster that are detected when it is located at  $z = 0.2$ .

results are shown in Fig. 8 where we also verify the good agreement of the analytic estimate of the variance given in Equation (24) with the one resulting from our Monte Carlo simulations.

We also use simulations to test the capability of the algorithm to estimate correctly the redshift of a cluster. The results are shown in Fig. 9. The mock clusters were composed requiring that they have 200 galaxies under the magnitude limit at  $z = 0.2$ . At higher redshifts, fewer galaxies are seen and analysed, explaining the increasing variance of the measurement. Note that even with single-band observations a redshift estimate for the clusters is possible albeit with larger errors with respect to the case in which the photometric redshift information is included. A similar result was obtained by Dietrich et al. (2007).

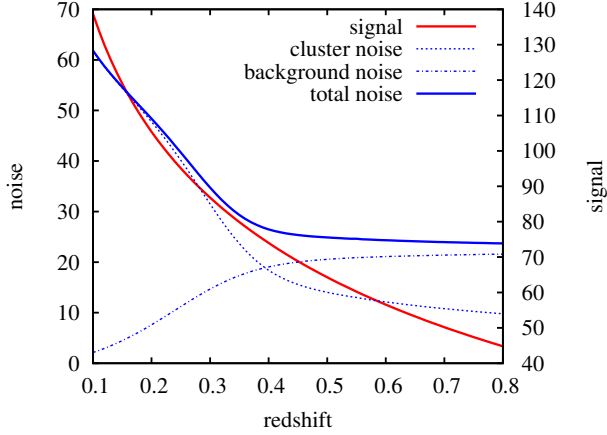


**Figure 6.** Signal and noise for a cluster with 100 visible galaxies at  $z = 0.2$  as a function of redshift. The signal (in red) corresponds to the number of galaxies below  $i' = 25$ , calculated from the model luminosity function. The dot-dashed line represents the noise due to the background galaxies, while the dashed line represents the noise due to the fluctuations in the cluster galaxy distribution. The solid blue line represents the total noise. Scales for noise and signal are shown on the left and right, respectively.

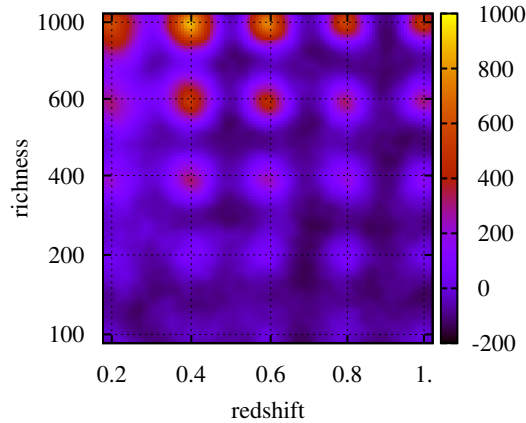


**Figure 7.** Distribution of the richness  $\Lambda$  at  $z_c = 0.4$ . Colorbar for  $\Lambda$  is reported on the right. The grid identifies the input positions of the mock clusters. The labels along the axes indicate the richness and redshift of the cluster at that position.

#### 4 OPTIMAL FILTER FOR WEAK LENSING

In the next Section we will apply to the COSMOS field both optimal filters for galaxy cluster detection from optical and weak lensing data. Here we introduce weak gravitational lensing and then the filtering method we will adopt for lensing data.

The observable quantity in weak lensing analyses is the reduced shear  $g$ , a measure of the distortion of background galaxies by intervening structures (i.e. galaxy clus-

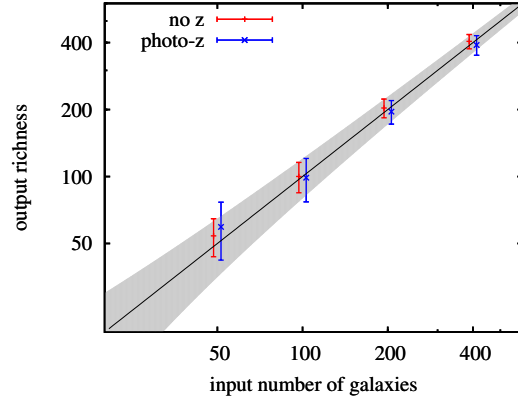


**Figure 8.** Calibration of the values for the richness  $\Lambda$  values obtained by the algorithm with and without redshift information. Clusters are located at  $z = 0.4$ . The shaded area represents the analytic estimate of the uncertainty, when the photometric redshift information is used.

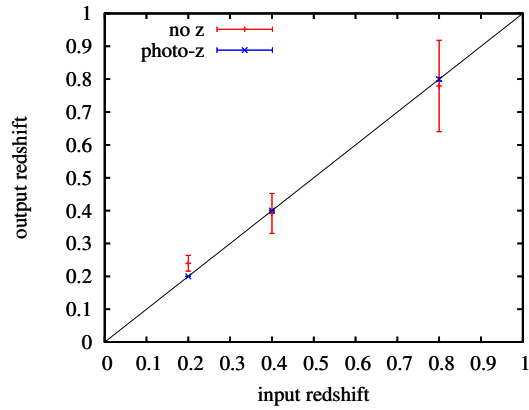


**Figure 9.** Redshift determination obtained by the algorithm, using the likelihood  $\mathcal{L}$  instead of the richness  $\Lambda$ , with and without redshift information. When photometric redshift are used, error bars become negligible.

ters). From the 2D projection of the cluster mass distribution,  $\Sigma(\theta)$ , one can calculate the lensing potential

$$\phi(\theta) = \frac{4G}{c^2} \frac{D_l D_s}{D_{ls}} \int d^2\theta' \Sigma(\theta') \ln |\theta - \theta'|, \quad (29)$$

where  $D_l$ ,  $D_s$  and  $D_{ls}$  are the angular diameter distances between lens and observer, source and observer, and lens and source, respectively. The complex reduced shear is then defined as

$$g(\theta) \equiv \frac{\gamma(\theta)}{1 - \kappa(\theta)}, \quad (30)$$

where the shear  $\gamma$  and the convergence  $\kappa$  are second-order derivatives of the lensing potential, namely

$$\kappa = \frac{1}{2}(\phi_{11} + \phi_{22}), \quad (31)$$

$$\gamma_1 = \frac{1}{2}(\phi_{11} - \phi_{22}), \quad (32)$$

$$\gamma_2 = \phi_{12}, \quad (33)$$



using the notation

$$\phi_{ij} = \frac{\partial^2 \phi}{\partial \theta_i \partial \theta_j}. \quad (34)$$

The linear matched filter for weak lensing cluster detections has been presented in Maturi et al. (2005). We refer the reader to that paper and to Pace et al. (2007) for a detailed description of its specific derivation, the comparison with other filtering techniques and tests of its performances. Here we summarise the main properties of the filter and how it can be applied to real data.

The weak lensing filter for cluster detection is expressed in Fourier space for convenience. Its shape is given by

$$\hat{\Psi}(\mathbf{k}) = \frac{1}{(2\pi)^2} \left( \int \frac{\hat{\tau}^2(\mathbf{k})}{P_N(k)} d^2k \right)^{-1} \frac{\hat{\tau}(\mathbf{k})}{P_N(k)}, \quad (35)$$

where  $\hat{\tau}$  is the Fourier transform of the weak lensing signal expected from a lensing cluster, i.e. the reduced shear, and  $P_N$  represents the power spectrum of the noise, due to the intrinsic ellipticity of the sources, their finite number on the sky and the additional shear induced by large-scale structures. The weak lensing signal model for clusters is computed assuming a spherically symmetric NFW density profile for the dark matter distribution (Equation 10). Again, as in the case of galaxy overdensities, the estimate of the lensing signal is obtained by convolving the shear data,  $D(\boldsymbol{\theta})$ , with the filter  $\Psi$ ,

$$A(\boldsymbol{\theta}) = \int D(\boldsymbol{\theta}') \Psi(\boldsymbol{\theta} - \boldsymbol{\theta}') d^2\theta'. \quad (36)$$

The variance of the estimate is

$$\sigma_A^2 = \frac{1}{(2\pi)^2} \int |\hat{\Psi}(\mathbf{k})|^2 P_N(k) d^2k. \quad (37)$$

The filter in Equation (35) was constructed requiring that the estimate of the amplitude of the signal  $A$  given by Equation (36) is unbiased and has minimum variance. The optical filter is the solution of the same problem for a galaxy distribution in magnitude and position. Note that if we neglect the noise contribution given by large-scale structures, i.e. we assume the noise to be white, this lensing filter and the one for the galaxy overdensities are fully equivalent, except of course for the specific nature of the two.

As in the case of the optical filter, the application of the weak lensing filter to the data is done evaluating  $A(\boldsymbol{\theta})$  over a grid of angular positions. Equation (36) is then discretized to be applied to real data. It becomes

$$A(\boldsymbol{\theta}) = \frac{1}{n_g} \sum_{k=1}^N \epsilon_{tk} \Psi(|\boldsymbol{\theta}_k - \boldsymbol{\theta}|), \quad (38)$$

where  $n_g$  is the number density of galaxies used for weak lensing measurement and  $\epsilon_{tk}$  denotes the tangential component of the  $k$ -th galaxy ellipticity with respect to the angular position. Thus, the filtering is performed in the real domain, which requires to back-Fourier transform the filter function defined in Equation (35). For every estimate of  $A$ , its error  $\sigma_A^2$  is also computed, according to Equation (37). Peaks with  $S/N > 3$  are selected from the map and considered as detections.

## 5 COSMOS FIELD

We now apply the optical filter and the weak lensing filter to the COSMOS field, a 2 square degree equatorial field that has been observed with the Hubble Space Telescope and with many other instruments, covering wavelengths from X-ray to radio (Scoville et al. 2007a).

### 5.1 Optical detections

For the optical analysis, we use the public galaxy catalogue with photometric redshifts (Ilbert et al. 2009), considering the angular position, the photometric redshift, and the  $i'$ -band magnitude measured with Subaru (Taniguchi et al. 2008). The photometric redshifts presented in the catalogue were obtained from the galaxy fluxes in 30 different bands, ranging from the ultraviolet to the near infrared. To each galaxy a SED has been assigned during the determination of the photometric redshift. We use this additional information to calculate the  $k$ -correction. We search for clusters between  $z = 0.1$  and  $z = 0.8$ , with steps of  $\Delta z = 0.02$ . The upper limit of  $z = 0.8$  is motivated by two factors: first, the model that we assume for the cluster luminosity function is based on low-redshift objects, and cannot be extrapolated to too high redshifts; second, if the  $k$ -correction becomes too strong for a given type of galaxies, our sample can no longer be assumed complete up to a given rest-frame magnitude. We scan an area smaller than the full field of view, such that, for each redshift, the filter (cut at  $r = 1$  Mpc/h) is completely inside the survey field. In this way we avoid any border effect, at the price of losing some possible detections of structures that have their centre inside the COSMOS area, but which are not completely contained in the field of view.

In Fig. 10, as examples, we show the results for the slices at  $z = 0.48, 0.50, 0.52$  where the detections with  $S/N > 3$  are marked with circles. Note that some structures are visible in more than one slice. In that case we assign as redshift of the detection the one where the likelihood is maximal, as discussed in Section 2.3. In this way we obtain 140 significant detections with a redshift estimate.

Since the absolute magnitude limit changes with redshift, the richness of clusters with the same galactic population is redshift dependent. In particular the richness decreases as the redshift increases. To correct for this effect and to obtain a quantity which depends on the cluster galaxy content only, we make use of the luminosity function  $\phi(m)$  of a cluster at an arbitrary redshift  $z_c = 0.2$  to compute the normalization factor

$$R(z) = \int_0^{m_{lim}(z)} \phi(m) dm. \quad (39)$$

This quantity represents the part of  $\phi(m)$  visible at a given redshift  $z$ . Dividing the measured richness  $\Lambda$  for  $R(z)$ , where  $z$  is the estimated redshift of the cluster, we obtain a value that is directly proportional to the physical galactic content of a cluster. More precisely this ‘corrected richness’ corresponds to the number of cluster galaxies that would be visible if the cluster was located at  $z = 0.2$ . The ‘corrected richness’ of our detections is shown in Fig. 11, together with the selection threshold  $S/N = 3$  for optical detections already derived and shown in the lower panel of Fig. 5. Notice

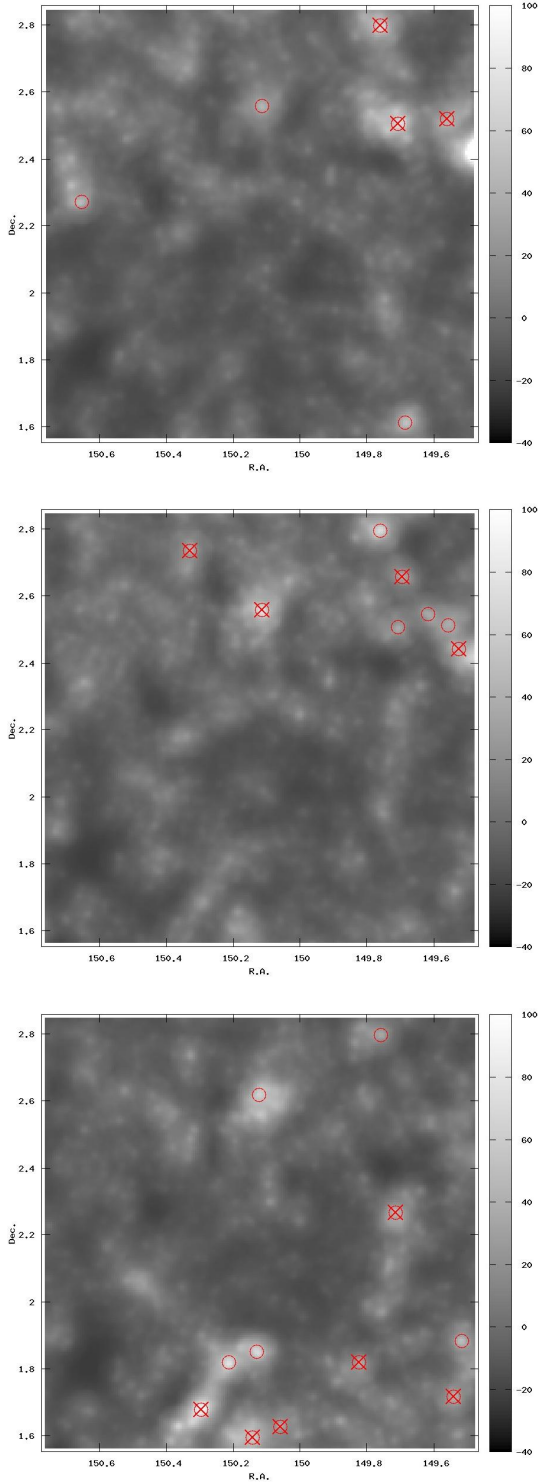


**Figure 10.** Maps of the estimates of the richness  $\Lambda$  on the COSMOS field, at redshifts  $z = 0.48, 0.5, 0.52$ , from top to bottom. Red circles indicate significant peaks, while red crosses represent a cluster detection at *that* redshift.

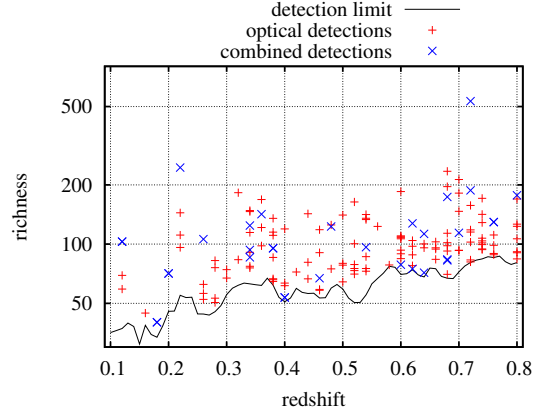


**Figure 11.** Redshift and (corrected) richness of the detected clusters. The black line represents the detection limit, that depends on model and field distributions at different redshifts. Clusters found in the optical analysis only are marked in red, those with a counterpart in the lensing analysis are marked in blue.

that the hills and wells of the curve are due to the change of the field population as a function of redshift.

## 5.2 Lensing detections

The weak lensing cluster detections in COSMOS are performed by applying Equation (38) as discussed by Maturi et al. (2005) on the shear catalogue obtained with the Suprime-Cam mounted on SUBARU (Miyazaki et al. 2007). The galaxy number density in the catalogue is  $42 \text{ arcmin}^{-2}$ . Following Miyazaki et al. (2007), we assume that the mean redshift of the sources is 0.8. The weak lensing cluster model used in the filter construction is the signal expected from a cluster of mass  $5 \times 10^{14} M_{\odot}$  at  $z = 0.5$ .

The total number of significant (e.g. with  $S/N > 3$ ) detections is 82. The expected number of spurious detections at this  $S/N$  level is around 40%, as computed by Pace et al. (2007). The derived weak lensing detections are related to the optical overdensities using a correlation length of 500  $\text{kpc}/h$ . This quite severe constraint is justified by the absence of any redshift information in the lensing data. The 27 detections satisfying this correlation criterion are listed in Table 1, while optical detections without a lensing counterpart are listed in the Appendix.

In Fig. 12 we show the redshift distribution of our combined detections. From the source redshift distribution it is possible to evaluate the redshift sensitivity function for weak lensing, that is a measurement of how much the shear of observed galaxies is sensitive to structures at different redshifts. In Fig. 12 we also show the optical sensitivity function, computed as the  $S/N$  of a cluster with 100 visible galaxies at  $z = 0.2$ . The ratio of lensing-confirmed clusters over the total number of optical detections in our analysis does not show any clear trend with redshift, but this could be due to the poor statistics.

## 5.3 Comparison with literature

We can compare our results to published catalogues of clusters previously extracted from the COSMOS field. Previous

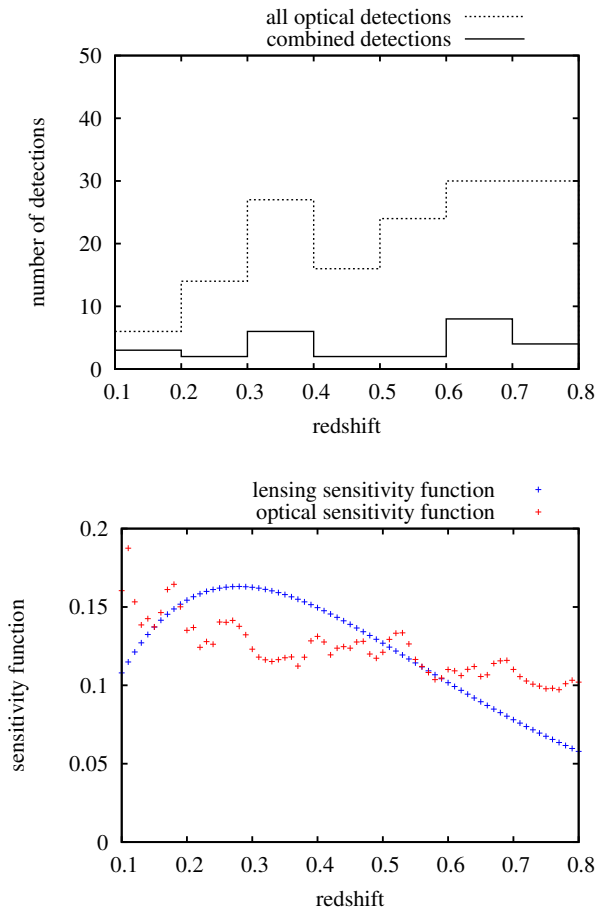


**Figure 12.** Top panel: redshift distribution of all optical detections (dashed line) and of the lensing-confirmed clusters (solid line). Bottom panel: lensing sensitivity function and optical sensitivity function, defined as the S/N of a cluster with 100 visible galaxies at  $z = 0.2$ , in arbitrary units.

analyses were done by Finoguenov et al. (2007), combining optical and X-ray information and by Olsen et al. (2007), who found galaxy overdensities, by applying a Postman-like filter to a previous version of the galaxy catalogue with no redshift information. Scoville et al. (2007b) analysed the COSMOS field with a wavelet method, and presented a catalogue of large-scale structures. We note that these structures are in general much larger than our targets, and that their size in some cases exceeds 10 Mpc in comoving coordinates. The few previous cluster detections in this field via lensing were reported by Kasliwal et al. (2008), while comparing the performance of ground-based and space-based telescopes for weak lensing, and by Miyazaki et al. (2007).

Correlating our detections with results from literature, we use different criteria depending on the characteristics of the catalogues. For sources presented in Finoguenov et al. (2007) and Olsen et al. (2007), we match detections using a physical correlation length of 1 Mpc/h, i.e. the cut-off applied to our radial filter. Instead, for the larger structures presented in Scoville et al. (2007b), we use a correlation length equal to the FWHM of their density peaks. In all these cases, the correlation along the line-of-sight is per-

ID	$z$	R.A.	Decl.	S/N	richness	previous detections
1	0.12	150.395	2.446	5.280	102.89	X
2	0.18	150.060	2.200	3.327	40.11	
3	0.20	150.616	2.425	3.802	70.95	X
4	0.22	150.192	1.650	6.628	244.74	XL
5	0.26	149.911	2.603	4.832	105.93	XSO
6	0.34	149.939	2.607	4.375	124.31	O
7	0.34	150.193	1.658	3.573	85.70	SL
8	0.34	150.299	1.609	3.749	93.49	XS
9	0.36	149.890	2.452	4.770	141.92	XS
10	0.38	150.142	2.053	3.831	95.29	
11	0.40	150.646	2.807	3.089	53.56	
12	0.46	150.687	2.400	3.419	67.07	
13	0.48	149.760	2.798	4.473	122.87	X
14	0.54	149.521	1.884	4.131	96.47	
15	0.60	149.926	2.519	3.202	78.57	L
16	0.62	149.572	1.882	3.018	74.84	S
17	0.62	150.590	2.473	4.035	127.47	
18	0.64	149.628	1.906	3.989	112.74	S
19	0.64	150.443	1.883	3.089	71.56	
20	0.68	149.718	1.816	3.428	82.65	
21	0.68	150.088	2.193	5.331	173.71	O
22	0.68	150.290	1.580	3.453	83.61	
23	0.70	150.308	2.406	3.975	114.17	S
24	0.72	149.921	2.521	8.721	532.42	XL
25	0.72	150.141	2.069	4.953	187.60	
26	0.76	150.641	2.804	3.764	129.46	S
27	0.80	150.437	2.763	4.705	177.08	S

**Table 1.** Catalogue of the clusters detected with both optical and lensing filters. The angular position is the one of the detection from optical data. In the last column we indicate whether the cluster has been found previously with other techniques: ‘X’ stands for Finoguenov et al. (2007), ‘S’ for Scoville et al. (2007b), ‘O’ for Olsen et al. (2007), ‘L’ for Kasliwal et al. (2008) or Miyazaki et al. (2007).

formed considering differences in redshift smaller than 0.05. This can be quite severe for Olsen et al. (2007), as their redshift determination was based on single band observations without any redshift information. For the lensing detections presented by Kasliwal et al. (2008) and Miyazaki et al. (2007), we use the same criterion we adopted for the internal matching with our lensing detections, i.e. a correlation length of 500 kpc/h. Regarding Finoguenov et al. (2007), we must stress that the comparison can only be done with their catalogue of X-ray confirmed clusters, obtained correlating 420 optical overdensities with 150 X-ray diffuse sources. This justifies some discrepancies between the two analyses.

The existence of previous detections of the objects found in our optical and lensing analysis is reported in the last columns of Tables 1 and A1.

We note here the ability of our optical filter to distinguish different galaxy clusters that are aligned along the line of sight, despite their signals are degenerate in weak lensing analyses. In fact, the two detections with identification numbers 4 and 7 correspond to SLJ1000.7+0137, a weak lensing and X-ray source studied by Hamana et al. (2009) with spectroscopical observations. They found that it is actually made by two, or possibly three, overdensities of galaxies at different redshifts, almost at the same angular position. Our method is able to disentangle the two structures

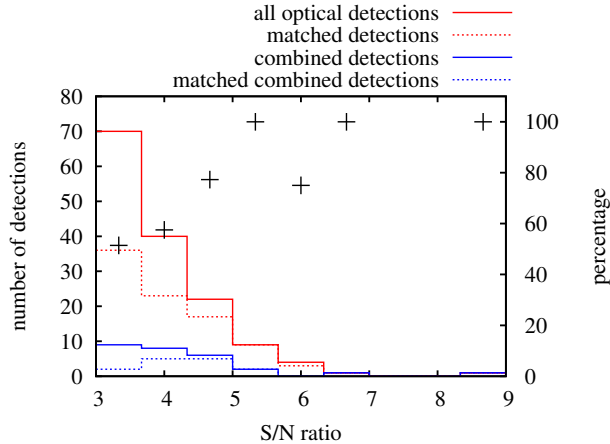


**Figure 13.** S/N distribution of all the significant optical detections (solid red), and of the detections with a counterpart in other analyses (dotted red). In blue we show the same distributions, but considering only combined (optical+lensing) detections. The black crosses indicate the percentage of our optical detections having at least one counterpart (scale on the right).

at  $z = 0.22$  and  $z = 0.34$  using information from photometric redshifts only. A similar case is that of SLJ1001.2+0135, described by Hamana et al. (2009) as the superposition of two overdensities, located at  $z = 0.22$  and  $z = 0.37$ . Our detection 8 corresponds to the latter, while at lower redshifts that angular position is outside the scanned area, because the filter would not be completely contained in the field of view (see Section 5.1). However, if we force our algorithm to analyse that region, we find an overdensity at  $z = 0.24$  with coordinates (R.A. = 150.329, Dec. = 1.609), confirming the alignment of two different structures.

#### 5.4 Characterizing our sample

In Fig.13 we plot the number of detections obtained with our analysis (both optical and optical plus lensing, dashed and solid lines respectively), as a function of their optical S/N ratio together with the corresponding amount of detections already reported in literature. As expected, the percentage of ‘matched’ detections increases as a function of S/N. The only detection with  $S/N > 5$  without a counterpart is actually near to a large structure observed by Scoville et al. (2007b) with a redshift mismatch of  $\Delta z = 0.06$ , only slightly larger than the limit we adopted.

To investigate the selection function of our method with respect to the mass, we plot in Fig. 14 the number of detections with respect to the X-ray masses estimated by Finoguenov et al. (2007). We include in this analysis only those X-ray clusters which lie inside the volume of our search, avoiding borders of the field and too high redshifts, as already discussed in Section 5.1. We see that the rate of X-ray clusters that are optically confirmed by our analysis increases with their mass, and it is above 50% for clusters of mass above  $1.5 \times 10^{13} M_{\odot}$ .

Finally we compare in Fig. 15 the corrected richness, corresponding to a measurement of the mass in galaxies, with the X-ray mass estimates made by Finoguenov et al.

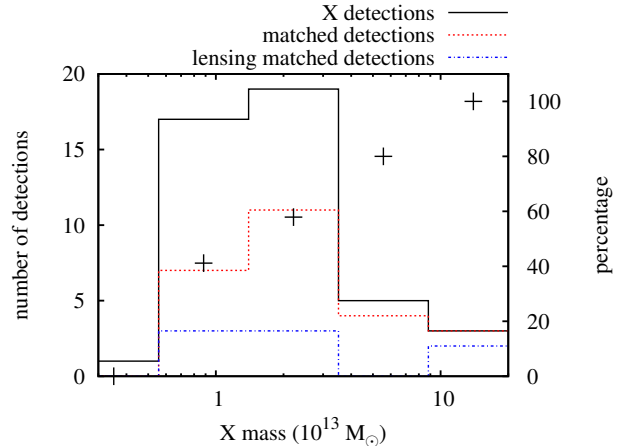


**Figure 14.** Mass distribution of all the X-ray detected clusters (in black), of the clusters we detect in the optical analysis (in red), and of those we detect in both optical and lensing analyses (in blue). The black crosses indicate the percentage of clusters detected in our optical analysis.

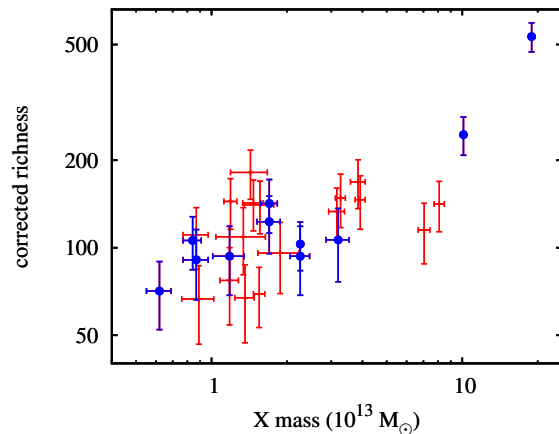


**Figure 15.** Correlation between the X-ray mass derived by Finoguenov et al. (2007) and our corrected richness. In red we show all the optical detections, in blue the lensing-confirmed clusters.

(2007). The proportionality between the two ‘mass estimates’ is clear although the scatter is very large. Note that the corrected richness is only a relative measure of the cluster stellar mass, in the sense that we do not quantify the physical mass scale. Note also that our filter has a fixed physical size, while the X-ray analysis was done inside an estimated  $r_{500}$  for each cluster, partially explaining the differences. The noise in the richness estimate for low-mass clusters is likely to be due to the field galaxies we observe inside our fixed spatial filter. This is expected given the error bars that show our analytic estimate.

## 6 SUMMARY AND CONCLUSIONS

In this paper we have presented an optimal linear filtering technique for the detection of galaxy clusters from optical and weak lensing data. The filter was first presented by Maturi et al. (2005) for weak lensing analysis and we now use the same formalism to extend it to optical data. The filter relies on a physical model for clusters and thus it accounts for all the known properties of galaxy clusters which can be inferred from photometric observations. Different information can be included and in this work we decided to restrict our analysis to the following observed properties of the galaxies: positions, magnitudes in one band, and photometric redshifts if present. The algorithm starts from a galaxy catalogue with the mentioned physical quantities and creates a map of values for the richness parameter  $\Lambda$  at different redshifts. The peaks of these maps represent the possible locations of galaxy clusters. The redshift of the clusters is determined by maximizing the likelihood of the data as a function of the redshift of the cluster model.

Our algorithm offers a number of improvements over existing filtering methods. Photometric redshifts are included in a flexible way, that adapts itself to the precision of the measurement of each galaxy, avoiding any sharp cut of the catalogue in redshift slices. It uses results from observed galaxy clusters to build a suitable model for cluster galaxy distributions. The richness calculated by the algorithm at the position of the cluster is a measurement of the number of galaxies in the detected cluster, that can be corrected for redshift dimming. Moreover, from the expected spatial profile and luminosity distribution of the clusters, and from the observed field population, it is possible to evaluate the noise of the detection and its significance. We tested the algorithm with numerical simulations, probing that it is able to obtain an unbiased estimate of the richness of the cluster, with an uncertainty predicted analytically from the model, and also its redshift.

We applied both the weak lensing and the optical filters to real data, obtaining a catalogue of candidate galaxy clusters for the COSMOS field. We presented a catalogue of 27 lensing-confirmed clusters, 11 of which do not have any previous detection in the literature. For the subsample of objects that have been analysed through their X-ray emission, we found that we are able to detect more than 50% of the clusters with an X-ray mass over  $1.5 \times 10^{13} M_{\odot}$  and we found a good correlation between our galaxy richness parameter and the cluster mass determined from X-ray temperature.

## APPENDIX A: OPTICAL-ONLY DETECTIONS

In Table A1 we list the optical detections without lensing counterpart.

## ACKNOWLEDGMENTS

We acknowledge financial contributions from contracts ASI-INAF I/023/05/0, ASI-INAF I/088/06/0, and ASI ‘EUCLID-DUNE’ I/064/08/0. This work was supported by the Transregio-Sonderforschungsbereich TR 33 of the

ID	$z$	R.A.	Decl.	S/N	richness	previous detections
28	0.12	149.862	1.765	4.279	69.35	X
29	0.12	150.432	2.630	3.925	59.13	
30	0.16	150.387	2.069	3.246	44.64	
31	0.22	150.102	2.358	5.042	144.29	XSO
32	0.22	150.395	2.460	4.397	111.20	O
33	0.22	150.620	2.707	4.070	96.12	S
34	0.26	149.842	2.682	3.436	56.19	S
35	0.26	150.089	2.474	3.640	62.42	
36	0.26	150.268	2.672	3.305	52.37	S
37	0.28	149.594	2.150	3.978	75.93	
38	0.28	149.969	2.450	3.190	50.52	S
39	0.28	150.044	2.225	4.159	82.51	SO
40	0.28	150.194	1.747	3.280	53.16	S
41	0.30	150.186	2.794	3.517	74.18	
42	0.30	150.572	1.942	3.337	67.24	X
43	0.32	150.456	2.049	5.332	182.39	S
44	0.32	150.652	2.313	3.531	83.32	S
45	0.34	149.596	2.820	4.773	146.29	XS
46	0.34	149.767	2.329	3.336	75.73	S
47	0.34	150.070	2.378	3.372	77.19	X
48	0.34	150.185	1.765	4.804	148.11	XS
49	0.34	150.373	2.444	3.691	90.87	XS
50	0.34	150.536	2.730	4.186	114.54	S
51	0.36	149.787	2.167	3.900	98.05	S
52	0.36	150.119	2.689	5.227	168.45	X
53	0.36	150.523	2.570	4.385	121.46	
54	0.38	149.675	2.413	3.133	66.70	S
55	0.38	149.767	1.625	3.112	65.94	
56	0.38	149.821	2.275	4.637	135.17	SO
57	0.38	149.966	1.678	4.250	115.08	X
58	0.38	150.234	2.474	3.609	85.62	
59	0.38	150.387	2.413	4.162	110.80	X
60	0.38	150.663	2.559	3.077	64.64	
61	0.40	149.578	2.533	3.343	61.52	
62	0.40	149.971	2.748	3.401	63.40	
63	0.40	150.356	2.651	4.816	119.47	
64	0.42	149.674	2.731	3.336	72.20	
65	0.44	149.961	2.210	3.315	66.64	XO
66	0.44	150.494	2.070	5.034	142.59	XSO
67	0.44	150.690	2.021	3.695	80.85	
68	0.46	149.667	1.625	4.658	118.42	S
69	0.46	150.354	2.741	3.178	58.86	
70	0.46	150.653	2.271	4.031	90.50	
71	0.46	150.721	2.244	3.160	58.26	
72	0.48	149.561	2.519	3.407	74.82	
73	0.48	149.707	2.506	4.519	125.21	S
74	0.50	149.525	2.441	3.519	78.18	S
75	0.50	149.695	2.657	3.148	64.27	
76	0.50	150.113	2.559	4.855	140.51	XS
77	0.50	150.328	2.735	3.562	79.87	S
78	0.52	149.542	1.719	3.733	73.37	
79	0.52	149.714	2.267	3.885	78.72	O
80	0.52	149.823	1.821	3.785	75.19	
81	0.52	150.059	1.629	3.646	70.42	
82	0.52	150.141	1.597	4.453	100.43	
83	0.52	150.295	1.680	5.809	163.77	
84	0.54	150.135	1.853	4.970	135.34	
85	0.54	150.216	1.821	4.928	133.21	X
86	0.54	150.260	1.765	3.528	72.84	
87	0.54	150.360	1.627	3.883	86.33	
88	0.54	150.467	2.066	5.088	141.32	X
89	0.54	150.573	2.166	3.591	75.14	

ID	$z$	R.A.	Decl.	S/N	richness	previous detections
90	0.56	149.525	1.760	4.173	123.00	
91	0.58	149.578	1.683	3.028	78.39	S
92	0.60	149.617	1.740	5.134	184.96	S
93	0.60	150.063	2.798	3.874	110.18	
94	0.60	150.253	2.346	3.334	84.34	
95	0.60	150.301	2.804	3.445	89.34	
96	0.60	150.491	2.745	3.851	109.03	X
97	0.60	150.574	2.608	3.827	107.78	
98	0.60	150.616	2.780	3.527	93.14	
99	0.60	150.717	2.537	3.799	106.39	
100	0.62	150.052	2.321	3.082	77.73	
101	0.62	150.520	2.473	3.620	104.23	
102	0.62	150.707	2.759	3.306	88.25	
103	0.62	150.725	2.625	3.492	97.54	
104	0.64	150.633	2.715	3.738	100.25	
105	0.64	150.737	2.825	3.644	95.81	X
106	0.66	149.802	1.804	3.204	83.66	S
107	0.66	150.185	2.158	3.438	94.33	
108	0.66	150.196	2.238	3.613	102.74	
109	0.66	150.687	1.667	3.469	95.77	
110	0.68	149.673	2.277	3.670	92.24	
111	0.68	149.925	2.597	3.092	70.21	S
112	0.68	149.948	2.097	4.162	113.53	
113	0.68	150.010	2.119	3.810	98.07	
114	0.68	150.060	2.608	6.305	234.42	SO
115	0.68	150.173	2.518	5.706	195.95	S
116	0.68	150.257	1.968	3.895	101.70	
117	0.70	149.647	2.828	3.514	93.08	
118	0.70	149.964	2.673	4.606	146.79	S
119	0.70	149.986	2.578	5.200	181.54	XSO
120	0.70	150.003	2.451	5.684	212.81	S
121	0.70	150.152	2.601	3.509	92.83	S
122	0.72	149.899	2.394	3.789	118.18	S
123	0.72	150.086	2.460	4.479	157.29	S
124	0.72	150.108	2.565	3.475	102.36	S
125	0.72	150.207	2.361	3.056	83.12	S
126	0.72	150.593	2.129	3.011	81.17	
127	0.72	150.736	2.416	3.731	115.19	S
128	0.74	149.523	2.656	3.344	101.46	
129	0.74	149.866	2.492	4.466	170.82	S
130	0.74	149.986	2.563	3.305	99.40	SO
131	0.74	150.024	2.688	3.388	103.83	S
132	0.74	150.051	2.302	3.821	128.61	S
133	0.74	150.116	2.705	4.030	141.57	SO
134	0.74	150.171	1.703	3.449	107.13	
135	0.74	150.296	2.378	3.196	93.72	S
136	0.74	150.547	2.803	3.212	94.55	S
137	0.76	149.559	1.647	3.054	88.26	
138	0.76	149.732	2.761	3.248	98.66	
139	0.76	149.839	1.684	3.468	111.29	
140	0.76	150.114	2.255	3.080	89.62	S
141	0.80	149.706	2.265	3.251	91.47	
142	0.80	150.040	2.652	3.906	126.31	
143	0.80	150.368	2.005	3.546	106.42	X
144	0.80	150.506	2.222	3.229	90.37	
145	0.80	150.538	2.148	3.097	84.12	O
146	0.80	150.580	2.652	4.594	169.49	S
147	0.80	150.702	2.769	3.850	123.09	

**Table A1.** As Table 1, but for clusters detected with the optical filter without lensing counterpart.

Deutsche Forschungsgemeinschaft. FB and TH thank the Institut für Theoretische Astrophysik of the University of Heidelberg for hospitality during the preparation of this work. We are grateful to M. Bartelmann for having carefully read the paper and provided useful comments. We also thank the anonymous referee for her/his interesting and stimulating remarks.

## REFERENCES

- Bartelmann M., 1996, *A&A*, 313, 697
- Dietrich J. P., Erben T., Lamer G., Schneider P., Schwobe A., Hartlap J., Maturi M., 2007, *A&A*, 470, 821
- Dong F., Pierpaoli E., Gunn J. E., Wechsler R. H., 2008, *ApJ*, 676, 868
- Finoguenov A., Guzzo L., Hasinger G., et al., 2007, *ApJS*, 172, 182
- Gilbank D. G., Bower R. G., Castander F. J., Ziegler B. L., 2004, *MNRAS*, 348, 551
- Gladders M., Yee H. K. C., 2000, *AJ*, 120, 2148
- Gladders M., Yee H. K. C., 2005, *AJ*, 157, 1
- Hamana T., Miyazaki S., Kashikawa N., Ellis R. E., Massey R. J., Refregier A., Taylor A., 2009, *PASJ*, 61, 833
- Hansen S. M., McKay T. A., Wechsler R. H., Annis J., Sheldon E. S., Kimball A., 2005, *ApJ*, 633, 122
- Hennawi J. F., Spergel D. N., 2005, *ApJ*, 624, 59
- Kasliwal M., Massey R., Ellis R., Miyazaki S., Rhodes J., 2007, *AAS*, 38, 927
- Kepner J., Fan X., Bahcall N., Gunn J., Lupton R., Xu G., 1999, *ApJ*, 517, 78
- Koester B. P., McKay T. A., Annis J., et al., 2007, *ApJ*, 660, 221
- Ilbert O., Capak P., Salvato M., et al., 2009, *ApJ*, 690, 1236
- Li H. I., Yee H. K. C., 2008, *AJ*, 135, 809
- Lu T., Gilbank D. G., Balogh M. L., Bognat A., 2009, *MNRAS*, 399, 1858
- Maturi M., Meneghetti M., Bartelmann M., Dolag K., Moscardini L., 2005, *A&A*, 442, 851
- Maturi M., Schirmer M., Meneghetti M., Bartelmann M., Moscardini L., 2007, *A&A*, 462, 473
- Mazure A., Adami C., Pierre M., 2007, *A&A*, 467, 49
- Menanteau F., Hughes J. P., Jimenez R., 2009, *ApJ*, 698, 1221
- Meneghetti M., Bartelmann M., Moscardini L., 2002, *MNRAS*, 340, 105
- Milkeraitis M., Van Waerbeke L., Heymans C., Hildebrandt H., Dietrich J. P., Erben T., 2009, *MNRAS*, 406, 673
- Miyazaki S., Hamana T., Shimazaki K., et al., 2002, *ApJ*, 580, 97
- Miyazaki S., Hamana T., Ellis R. S., Kashikawa N., Massey R. J., Taylor J., Refregier A., 2007, *ApJ*, 669, 714
- Navarro, J. F., Frenk C. S., White S. D. M., 1997, *ApJ*, 618, 557
- Olsen L. F., Benoist C., Cappi A., et al., 2007, *A&A*, 461, 81
- Pace F., Maturi M., Meneghetti M., Bartelmann M., Moscardini L., Dolag K., 2007, *A&A*, 471, 731
- Pace F., Maturi M., Bartelmann M., Cappelluti N., Dolag K., Meneghetti M., Moscardini L., 2008, *A&A*, 483, 389
- Popesso P., Böhringer H., Romaniello M., Voges W., 2005, *A&A*, 433, 415
- Postman M., Lubin L. M., Gunn J. E., Oke J. B., Hoessel J. G., Schneider D. P., Christensen J., 1996, *AJ*, 111, 615
- Ramella M., Boschin W., Fadda D., Nonino M., 2001, *A&A*, 368, 776
- Schäfer B. M., Pfrommer C., Hell R. M., Bartelmann M., 2006, *MNRAS*, 370, 1713
- Schechter P., 1976, *ApJ*, 203, 297
- Schirmer M., Erben T., Schneider P., Wolf C., Meisenheimer K., 2004, *A&A*, 420, 75
- Schneider P., van Waerbeke L., Jain B., Kruse G., 1998, *MNRAS*, 296, 873
- Scoville N., Aussel H., Brusa M., et al., 2007, *ApJS*, 172, 1
- Scoville N., Aussel H., Benson A., et al., 2007, *ApJS*, 172, 150
- Springel V., White S.D.M., Jenkins A., et al., 2005, *Nat*, 435, 629
- Taniguchi Y., Scoville N., Murayama T., et al., 2008, *ApJS*, 172, 9
- Thanjavur K., Willis J., Crampton D., 2009, *ApJ*, 706, 571